Relaxation time spectrum of low-energy excitations in one- and two-dimensional materials with charge or spin density waves

S. Sahling,[1,2] G. Remenyi,[2,3] J. E. Lorenzo,[2] P. Monceau,[2] V. L. Katkov,[4] and V. A. Osipov[4]

[1]*Institut für Festkörperphysik, Technische Universität Dresden, 01062 Dresden, Germany*

[2]*Centre National de la Recherche Scientifique, Institute Néel, F-38042 Grenoble, France*

[3]*Université Grenoble Alpes, Institute Néel, F-38042 Grenoble, France*

[4]*Bogoliubov Laboratory of Theoretical Physics, Joint Institute for Nuclear Research, 141980 Dubna, Moscow region, Russia*

(Received 18 June 2016; published 24 October 2016)

The long-time thermal relaxation of $(TMTTF)_2Br$, $Sr_{14}Cu_{24}O_{41}$ and $Sr_2Ca_{12}Cu_{24}O_{41}$ single crystals at temperatures below 1 K and magnetic field up to 10 T is investigated. The data allow us to determine the relaxation-time spectrum of the low-energy excitations caused by the charge-density wave or spin-density wave (SDW). The relaxation time is mainly determined by a thermal activated process for all investigated materials. The maximum relaxation time increases with increasing magnetic field. The distribution of barrier heights corresponds to one or two Gaussian functions. The doping of $Sr_{14-x}Ca_xCu_{24}O_{41}$ with Ca leads to a drastic shift of the relaxation-time spectrum to longer time. The maximum relaxation time changes from 50 s ($x = 0$) to 3000 s ($x = 12$) at 0.1 K and 10 T. The observed thermal relaxation at $x = 12$ clearly indicates the formation of the SDW ground state at low temperatures.

DOI: 10.1103/PhysRevB.94.144107

I. INTRODUCTION

Low-energy excitations exist in low dimensional systems [one-dimensional (1D) or two-dimensional (2D)] with charge-density wave (CDW) or spin-density wave (SDW) with a broad spectrum of relaxation time. This leads to a nonexponential thermal relaxation and an additional contribution to the heat capacity below 1 K which strongly depends on the time and magnetic field [1–5].

It was not possible to determine the equilibrium heat capacity of this contribution in materials with incommensurate CDW or SDW up to now, since the maximum of the relaxation-time spectrum was too long in comparison to the time window of the experiment [5]. This was achieved for the first time with the commensurate 1D SDW compound $(TMTTF)_2Br$ by extending the time window of the measurement up to 22 000 s [6,7]. It was shown that the equilibrium heat capacity is strongly proportional to T^{-2} corresponding to an upper tail of a Schottky term with a magnetic field dependent Schottky energy E_s. The end of the inner relaxation $t_{\rm in}$ was obtained as a function of the temperature and magnetic field. The experimental parameter $t_{\rm in}$ is close to the maximum value of the relaxation-time spectrum. It follows the Arrhenius law:

$$t_{\rm in} = \tau_0 \exp\left(\frac{E_a}{k_B T}\right), \tag{1}$$

with an activation energy $E_a/k_B = 0.5$ K that does not depend on the magnetic field H while the parameter τ_0 is found to be proportional to H^2 at large H. The maximum of the Schottky term always occurs at too low temperatures to be observed in this experiment.

It should be noted that the long-time thermal measurements have proven highly effective in studies of the ground-state structure of a variety of materials at very low temperatures. In particular, a recent experiment [8] reports the observation of the sharp heat capacity increase in pyrochlore oxide $Dy_2Ti_2O_7$ below 0.4 K that has not previously been detected. This led to a conclusion that the ground state of thermally equilibrated $Dy_2Ti_2O_7$ might correspond to the onset of order instead of the expected degenerate manifold of spin-ice states.

A new group of materials is $Sr_{14-x}Ca_xCu_{24}O_{41}$ where a 2D CDW is formed after an insulator-to-insulator transition unlike the standard systems where electron density waves (DWs) appear at temperatures below a metal-to-insulator transition. Increasing the Ca content destroys the order so that the CDW disappears completely for $x \geqslant 11.5$. Notice that CDW dynamics in these materials has been intensively studied by using different experimental techniques including dc and electric-field dependent transport, various spectroscopic methods, low-frequency electronic Raman scattering, and resonant x-ray diffraction (for details, see Ref. [9] and the references therein).

Recently [10], the heat capacity was investigated for $x = 0$ and 12. The equilibrium heat capacity and the parameter $t_{\rm in}$ were obtained for both materials as a function of the temperature and magnetic field. For the material without Ca, the Schottky contribution was found including the presence of the maximum of the Schottky term. A surprising result was obtained for $t_{\rm in}$ which proved much shorter compared to other investigated materials. In a Ca-doped sample ($x = 12$), the Schottky term was also observed but with significantly longer $t_{\rm in}$. The maximum relaxation time of the spectrum was determined in all these experiments only. An interesting question is, how does the whole relaxation-time distribution function look out? The aim of our paper is to answer this question.

II. EXPERIMENT

The relaxation-time spectrum and the equilibrium heat capacity can be obtained by the relaxation-time method. First, a constant heater power changes the sample temperature after the waiting time $t_w = 2t_{\rm in}$ to the new equilibrium temperature T_1. Then the heater power is switched off at $t = 0$ and the temperature is measured as a function of time. The equilibrium

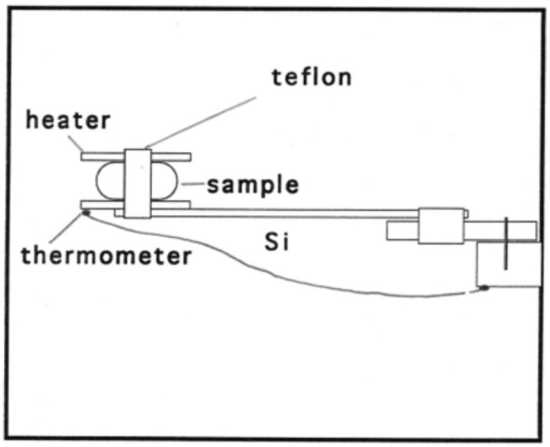

FIG. 1. Schematic picture of the experimental setup.

relaxation time τ_{eq} can be obtained for $t > t_{in}$ (see Fig. 1) and we can determine the heat capacity $C_p = \tau_{eq}/R_{hl}$ with $R_{hl} = (T_1 - T_0)/(U_h I_h)$ being the thermal resistance between the sample and the sample holder, U_h the heater voltage, and I_h the heater current.

The distribution function of the relaxation times $G(\ln\tau)$ can be recovered from the temperature dependence at short times $t < t_{in}$, which can be expressed as [11]

$$\frac{\Delta T_i}{\Delta T_0} = \int_{\ln\tau_{min}}^{\infty} G(\ln\tau)\exp\left(-\frac{t}{\tau}\right)d\ln\tau, \tag{2}$$

where τ_{min} is a short-time cutoff,

$$\Delta T_i(t) = \Delta T(t) - \Delta T_{eq}, \tag{3}$$

and

$$\Delta T_{eq} = \Delta T_{eq}^0 \exp\left(-\frac{t}{\tau_{eq}}\right). \tag{4}$$

Namely, we subtract from the measured temperature difference at given time its extrapolated quasiequilibrium value. Notice that this procedure brings additional numerical error which, together with the error in measurements, does not exceed 10% for $\Delta T_i(t)$. A similar estimate is valid for all extracted parameters.

We are looking for a distribution function of $\ln\tau$, which corresponds to a distribution of the barrier heights in the case of thermal activation or tunneling process. We will show that the data of all investigated materials can be calculated with one or two Gaussian distribution functions. We get reasonable results only if we measure the time dependence of the temperature relaxation longer than t_{in}, which means that $\tau_{eq} = R_{hl}C_p$ must be longer than t_{in}. For this reason, we have to choose a very large heat link R_{hl} and sample mass. On the other side, the maximum time of measurements is limited by the fluctuation of temperature caused by fluctuation of the parasitic heat flow:

$$\Delta T(t_{max}) = \Delta T_{fl} = R_{hl}\Delta P_{par}. \tag{5}$$

The experiment required a very low value of the parasitic heat flow fluctuations during a long time. ΔP_{par} was in our experiments between 1 and 10 pW. This leads to a temperature fluctuation in a range between 10 and 100 μK, where an optimal heat leak of 10^7 K/W at 0.1 K was used. To realize the heat link the sample was mounted together with a heater and a self-made AuGe thermometer [12] on the end of a thin Si platelet ($30 \times 4 \times 0.2$ mm^3), which gives a heat link of 10^8 at 0.1 K. The heat link is then reduced by a $30 - \mu$m Cu wire on the thermometer. The sample was in the form of a sandwich: heater-sample-thermometer-heat link. All together was fixed by small Teflon threads and grease. The addenda was measured separately. The schematic picture of the device is shown in Fig. 1. In all experiments single crystals were used with masses 64 mg $(TMTTF)_2Br$, 440 mg ($Sr_{14}Cu_{24}O_{41}$), and 2082 mg ($Sr_2Ca_{12}Cu_{24}O_{41}$).

III. RESULTS

A. $(TMTTF)_2Br$

Figure 2 shows the thermal relaxation from $T_1 = 102$ mK to $T_0 = 92$ mK after a constant power of the sample heater is switched off at $t = 0$ at different magnetic field. The magnetic field was directed along the c axis (parallel to the SDW). The waiting time of the constant power was $2t_{in}$, so that we start from the equilibrium state at temperature T_1. The temperature difference $\Delta T_0 = T_1 - T_0$ was between 5 and 10% of T_0. The nonexponential dependence of the time at the beginning is caused by the inner relaxation process, which is finished at t_{in} (arrows in Fig. 2). At longer time the thermal relaxation follows Eq. (4) (strait lines) and the parameters ΔT_{0eq} and τ_{eq} can be determined. The relaxation time τ_{eq} yields together with the corresponding heat link the equilibrium heat capacity, which is in good agreement with our earlier results [6,7]. Another presentation of the thermal relaxation is given in Fig. 3. It is seen that the maximum value of ΔT_{0eq} is about 5–7% of the total ΔT_0. This means that we have less than 0.7 mK to determine the exponential relaxation law and the equilibrium heat capacity at 0.1 K.

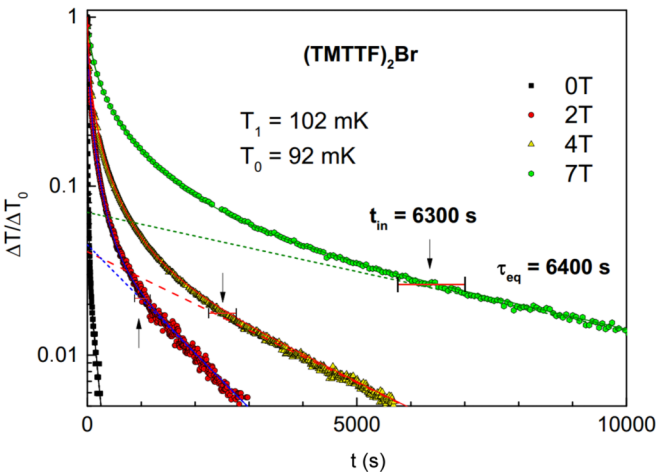

FIG. 2. A constant power of the sample heater is switched off at $t = 0$ after the waiting time $t_w = 2t_{in}$ and the temperature relaxes from $T_1 = 102$ mK to $T_0 = 92$ mK. The inner relaxation is finished after the time t_{in} (arrows). The thermal relaxation follows Eq. (4) at longer time $t > t_{in}$ (straight lines). The quasiequilibrium relaxation time τ_{eq} and the end of the inner relaxation t_{in} depend strongly on the magnetic field.

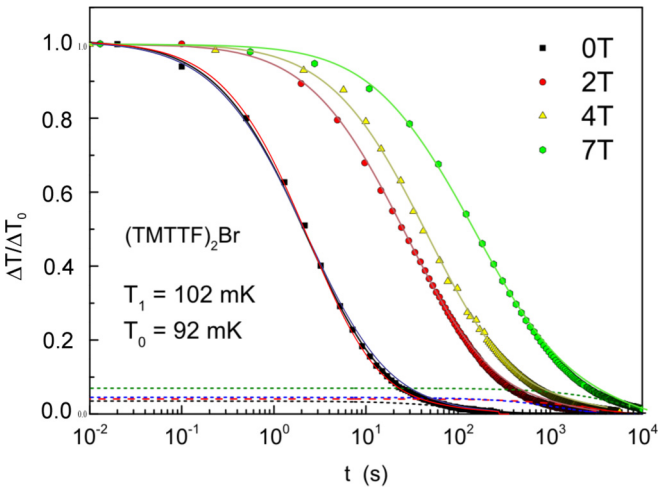

FIG. 3. The data of Fig. 2 in the semilog presentation. The straight lines of Fig. 2 (quasiequilibrium relaxation) are shown by the dashed curves. More than 90% of the measured initial temperature difference is caused by the inner relaxation process. The solid lines are calculated by Eqs. (2)–(4) with a Gaussian distribution function. Two fitting parameters of this distribution function τ_m (the position of the maximum) and w (the width of the distribution) are given in Table I and Fig. 5 for $T_0 = 0.092$ K. For zero field, two additional fitting curves show the cases of $1.1w$ (blue) and $0.9w$ (red).

The process of relaxation is generally characterized by the relaxation rate:

$$S(t) = \frac{d}{d\ln t}\left(\frac{\Delta T_i}{\Delta T_0}\right). \tag{6}$$

Differentiation of the right side in Eq. (2) with respect to $\ln t$ converts the kernel of integration $\exp(-t/\tau)$ to a peak $-\exp(-e^{\ln t-\ln\tau} + \ln t - \ln\tau)$ with a center at $\ln t$, the height $1/e$, and the width of approximately e in the scale of $\ln\tau$. In the case where $G(\ln\tau)$ changes slowly, the peak may be considered as a δ function, so that $G(\ln t) = S(\ln t)$. It is quite appropriate to describe data for $(TMTTF)_2Br$. However, if $G(\ln t)$ is a rapidly varying function, $S(t)$ gives the broadened distribution of relaxation times. As will be shown, this occurs in the other two materials where the distribution functions look like sharp peaks. For this reason, in order to obtain $G(\ln\tau)$ properly we use another procedure. Namely, we assume that $G(\ln\tau)$ is given by a Gaussian distribution

$$G_i(\ln\tau) = \frac{A_i}{w_i\sqrt{2\pi}}\exp\left(-\frac{\ln^2(\tau/\tau_{mi})}{2w_i^2}\right), \tag{7}$$

where $A_i = \Delta T_i/\Delta T_0$ at $t = 0$. Then we replace the integral in Eq. (2) by a finite sum. As a result, one gets a polynomial $R(t,\tau_{mi},w_i)$ with t being a variable and τ_{mi} and w_i the fitting parameters. These parameters are determined to provide a best fit of $R(t,\tau_{mi},w_i)$ to the experimental data for $\Delta T_i(t)/\Delta T_0$ in Fig. 3. The result is given in Table I. As a proof, we substitute Eq. (7) with extracted τ_{mi} and w_i to the right-hand side of Eq. (2). The result of numerical integration is shown in Fig. 3 by solid lines. Notice that the relative error is found to be less than 3% in all considered cases.

TABLE I. Parameters of the Gaussian distribution for $(TMTTF)_2Br$. Estimated errors for the given values are 10%.

$\mu_0 H$	0 T	2 T	4 T	7 T
A_i	0.965	0.955	0.959	0.93
w_i	1.16	1.35	1.37	1.46
$\tau_{mi}(s)$	3.0	36	64.9	196

As is seen in Fig. 4, the measured relaxation rate becomes slightly broadened as compared to calculated $G(\ln\tau)$ while the position of the maximum is almost identical. To illustrate the sensitivity of the fitting procedure to the parameter w_i, the additional curves with a 10% shift of the width of the distribution are shown in Fig. 3 for zero field: $0.9w_i$ (red line) and $1.1w_i$ (blue line). Similar deviations are found for nonzero fields.

Parameters $t_{\rm in}$ and τ_{mi} have the same magnetic field dependence

$$t_{\rm in} = t_{\rm in}(0) + B_i(\mu_0 H)^2, \tag{8}$$

$$\tau_{mi} = \tau_{mi}(0) + C_i(\mu_0 H)^2, \tag{9}$$

where $t_{\rm in}(0) = 2.5\alpha$ s, $B_i = 0.46\alpha$ s T^{-2}, $\tau_{mi}(0) = 0.05\alpha$ s, $C_i = 0.015\alpha$ s T^{-2}, and $\alpha = \exp[0.51(\mathrm{K})/T]$. The values are given for the field induced phase (see Ref. [7]). Meanwhile, the width of the distribution increases weakly linearly (see Fig. 5).

We have also determined the spectrum for different temperatures and fixed magnetic field. The result is the same as for $t_{\rm in}$ in Ref. [7]: maximum values follow the Arrhenius law with the activation energy $E_a/k_B = 0.51$ K. E_a does not depend on the magnetic field.

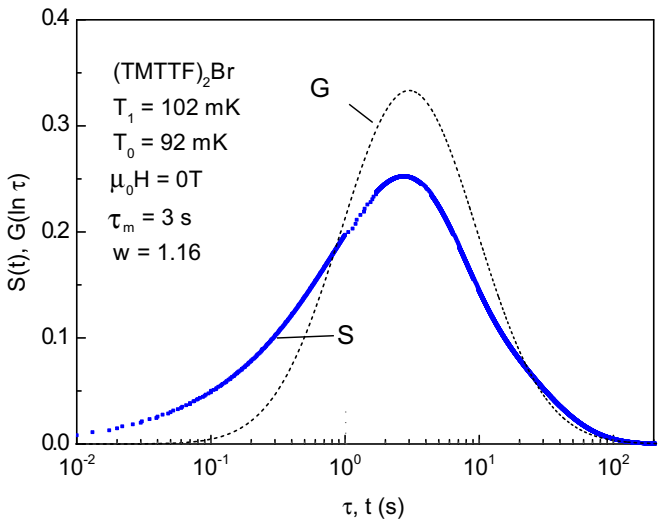

FIG. 4. The measured inner thermal relaxation $\Delta T_i/\Delta T_0$ in the presentation $d(\Delta T_i/\Delta T_0)/d(\ln t)$ as a function of time (blue points) for the data shown in Figs. 2 and 3. This gives roughly the distribution function of relaxation time (see the text). The numerical calculation of $\Delta T_i/\Delta T_0$ with Eq. (2) yields a Gaussian distribution (dashed curve) with nearly the same position of the maximum τ_m.

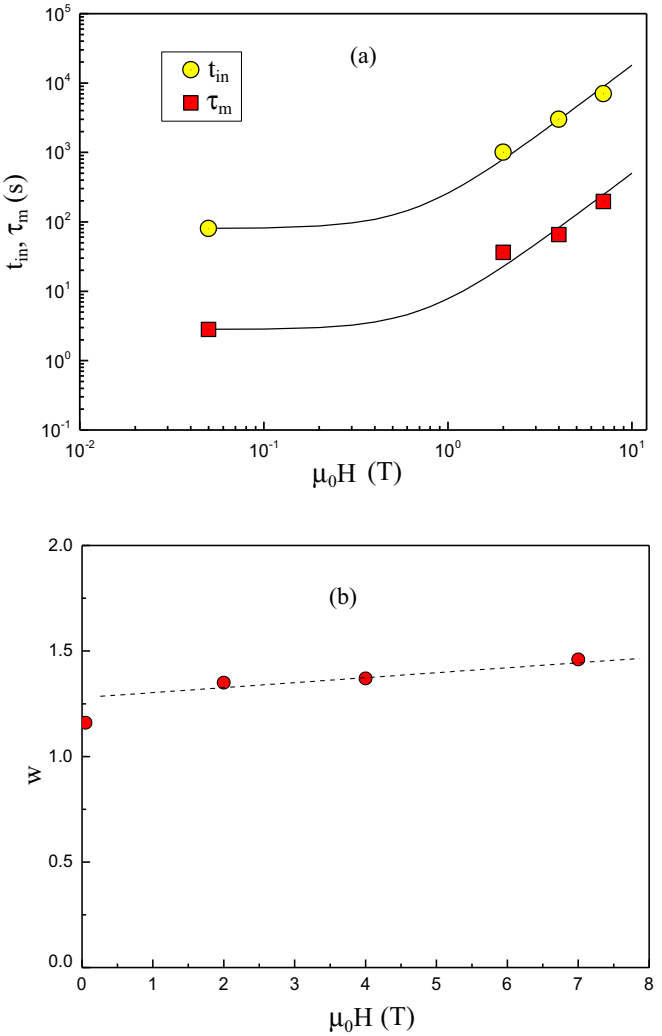

FIG. 5. Equation (2) yields a good fit to the inner thermal relaxation $\Delta T_i(t)$ when a Gaussian distribution function of relaxation time is used. The obtained fitting parameters τ_m (the position of the maximum) and w (the width of the distribution) are shown in Figs. 5(a) and 5(b) for the data of Fig. 3 ($T_0 = 0.092$ K and different magnetic field). Figure 5(a) also shows the time t_{in} (for $t > t_{in}$ the inner relaxation can be neglected, see Figs. 2 and 3). τ_m and t_{in} are proportional to H^2 at high magnetic field, i.e., with increasing magnetic field the distribution function is shifted to higher values without change of the distribution width. The error corresponds to the size of symbols.

B. $Sr_{14}Cu_{24}O_{41}$

The heat capacity was measured by pulse technique in both a very short- (30 ms) and long-time range with $\tau_{eq} > t_{in}$. The magnetic field was directed along the c axis.

The upper curves in Fig. 6 present the total equilibrium heat capacity including the Schottky term caused by the CDW. The contribution of the CDW can be completely excluded in the short-time experiment thus allowing us to determine the background heat capacity (see Fig. 6). In contrast to $(TMTTF)_2Br$, there are many other (fast) contributions including 1D bosons [13], which will be presented and discussed in a separate paper [10]. The CDW contribution

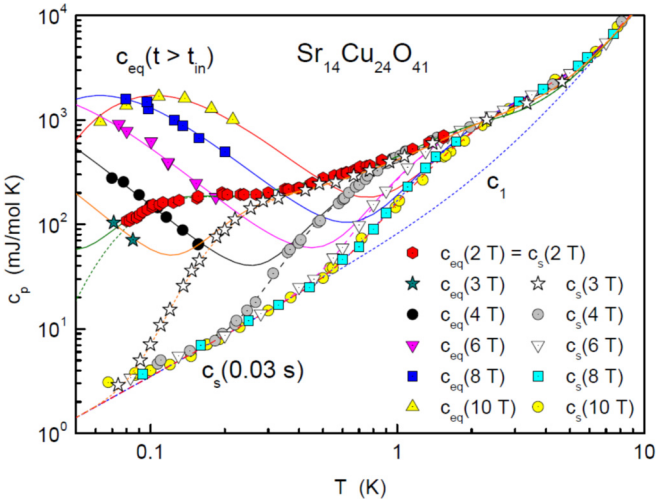

FIG. 6. The heat capacity of $Sr_{14}Cu_{24}O_{41}$ as a function of the temperature for different magnetic fields measured at very short time ($t = 30$ ms) and long time ($t > t_{in}$). The CDW does not contribute to the short-time heat capacity. The solid lines show the total equilibrium heat capacity at different magnetic field. Below 0.3 K it is determined by a magnetic field independent quasilinear term (dashed line) and a Schottky contribution. The Schottky energy is proportional to H^2.

is small in comparison to the background below 3 T. The maximum of the Schottky term was first observed in a magnetic field of 10 T. The amplitude A_s is equal to 3.9 J/mol K. This value is essentially smaller in comparison to $(TMTTF)_2Br$ where the estimated upper limit is about 50 J/mol K. The

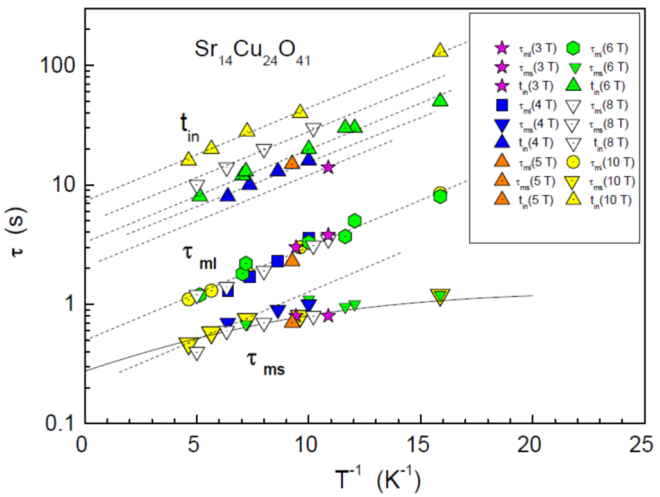

FIG. 7. The end of the inner thermal relaxation t_{in} (see also Fig. 8) follows the Arrhenius law [Eq. (1)] with a magnetic field independent activation energy $E_a/k_B = 0.2$ K. The absolute value depends weakly on the magnetic field. Two Gaussian distribution functions of relaxation time are necessary to calculate the inner relaxation $\Delta T_i(t)$ [according to Eq. (2)] with the maximum at τ_{ms} and τ_{ml} (see also Fig. 9). Both parameters are magnetic field independent, i.e., the increase of t_{in} at fixed temperature and increasing magnetic field is a consequence of an increasing width. The temperature dependence of τ_{ml} corresponds to Eq. (1) with the same activation energy as for t_{in}. The temperature dependence of the shorter τ_{ms} deviates from Eq. (1) at low temperatures. The solid line is obtained when we include in addition a tunneling process [see Eqs. (10)–(12)].

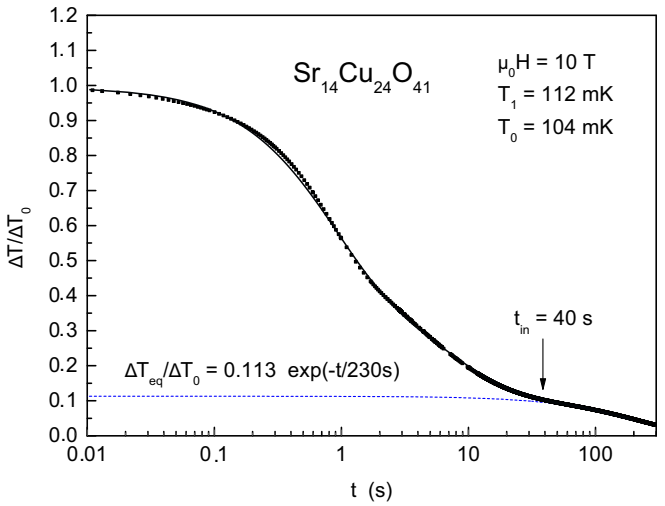

FIG. 8. A constant power of the sample heater is switched off at $t = 0$ after the waiting time $t_w = 2t_{\rm in}$ and the temperature relaxes from $T_1 = 112$ mK to $T_0 = 104$ mK. The inner relaxation is finished after the time $t_{\rm in}$ (the arrow). The thermal relaxation follows Eq. (4) at longer time $t > t_{\rm in}$ (dashed curve). The solid line shows the result of the calculation $(\Delta T_{\rm eq} + \Delta T_i)/\Delta T_0$ where ΔT_i is obtained from Eq. (2) with two Gaussian functions in Fig. 9 (dashed lines).

Schottky energy is equal to 250 mK at 10 T and varies with the magnetic field as H^2.

The most surprising result is associated with $t_{\rm in}$, which was determined in good agreement with the pulse and relaxation-time method (see Fig. 7). The inner relaxation is finished at 0.1 K and 10 T even after 40 s while the expected value for $(TMTTF)_2Br$ is 20 000 s (10 000 s at 7 T). The temperature dependence again meets the Arrhenius law with a

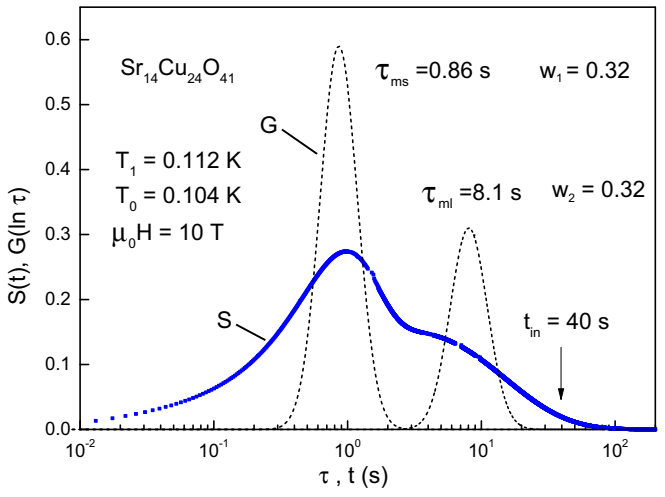

FIG. 9. The measured inner thermal relaxation $\Delta T_i/\Delta T_0$ in the presentation $d(\Delta T_i/\Delta T_0)/d(\ln t)$ as a function of time (blue points) for the data shown in Fig. 8. This gives roughly the distribution function of relaxation time (see the text). The numerical calculation of $\Delta T_i/\Delta T_0$ with Eq. (2) yields two Gaussian distributions (dashed curve). The corresponding four fitted parameters are shown. The positions of the peaks do not depend on the magnetic field (see Fig. 7).

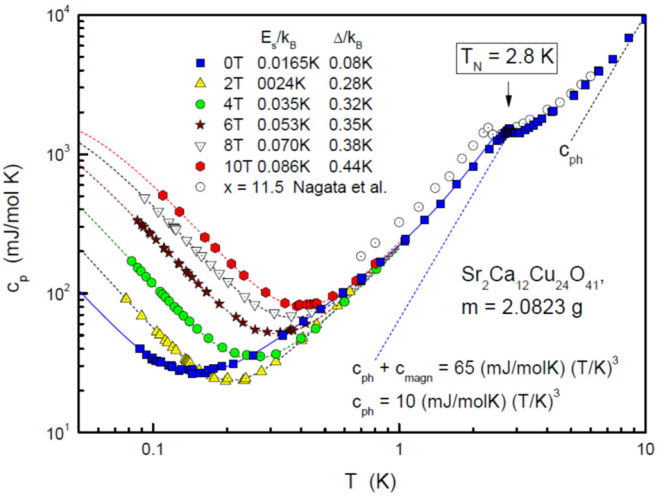

FIG. 10. The heat capacity of $Sr_2Ca_{12}Cu_{24}O_{41}$ measured at long time $t > t_{\rm in}$ as a function of the temperature for different magnetic field. Antiferromagnetic ordering is observed at 2.8 K. The heat capacity is determined below the transition by a T^3 term (magnons and phonons), quasilinear term with a magnetic field dependent gap, and the Schottky term which is strongly time dependent for $t < t_{\rm in}$. The values of the gap Δ and Schottky energy E_s for different magnetic field are given in the inset. The solid lines show the calculated equilibrium heat capacity, which is determined below 0.3 K by the quasilinear term and the Schottky contribution only.

smaller activation energy $E_a/k_B = 0.2$ K. The magnetic field dependence is less strong: the value of $t_{\rm in}$ is changed three times only with increasing magnetic field from 4 to 10 T.

Figure 8 shows the thermal relaxation after switching off a constant power of the sample heater ($T_1 = 112$ mK, $T_0 = 104$ mK, $\mu_0 H = 10$ T). The exponential relaxation is observed for $t > 40$ s. The extrapolation to $t = 0$ gives a maximum of $\Delta T_{\rm eq}$ which is estimated as 12% of the total temperature difference ΔT_0. Thus, for the determination of both $\tau_{\rm eq}$ and equilibrium heat capacity remains less than 1 mK. The other 88% of ΔT is caused by the inner relaxation process (see Fig. 7). The same procedure as described above gives us the rough relaxation-time spectrum (points in Fig. 9) and the best approximation of the relaxation-time spectrum in the form of two Gaussian functions (dashed curves in Fig. 9).

The investigation of the magnetic field dependence at fixed temperature yields the next surprise: the positions of two distribution peaks do not change in the magnetic field. The upper distribution function becomes only broader and is responsible for a magnetic field dependence of $t_{\rm in}$. The lower Gaussian function becomes unchanged in the magnetic

TABLE II. Parameters of the temperature relaxation in $Sr_2Ca_{12}Cu_{24}O_{41}$ that are given by the expression $\Delta T_i/\Delta T_0 = A_i \exp[-(t/\tau_{mi})^{0.9}]$, $T_0 = 0.1$ K, $m = 2.0823$ g. Estimated errors for the given values are 10%.

$\mu_0 H$	0 T	3 T	6 T	10 T
A_i	0.81	0.81	0.81	0.81
$\tau_{mi}(s)$	63	143	252	543

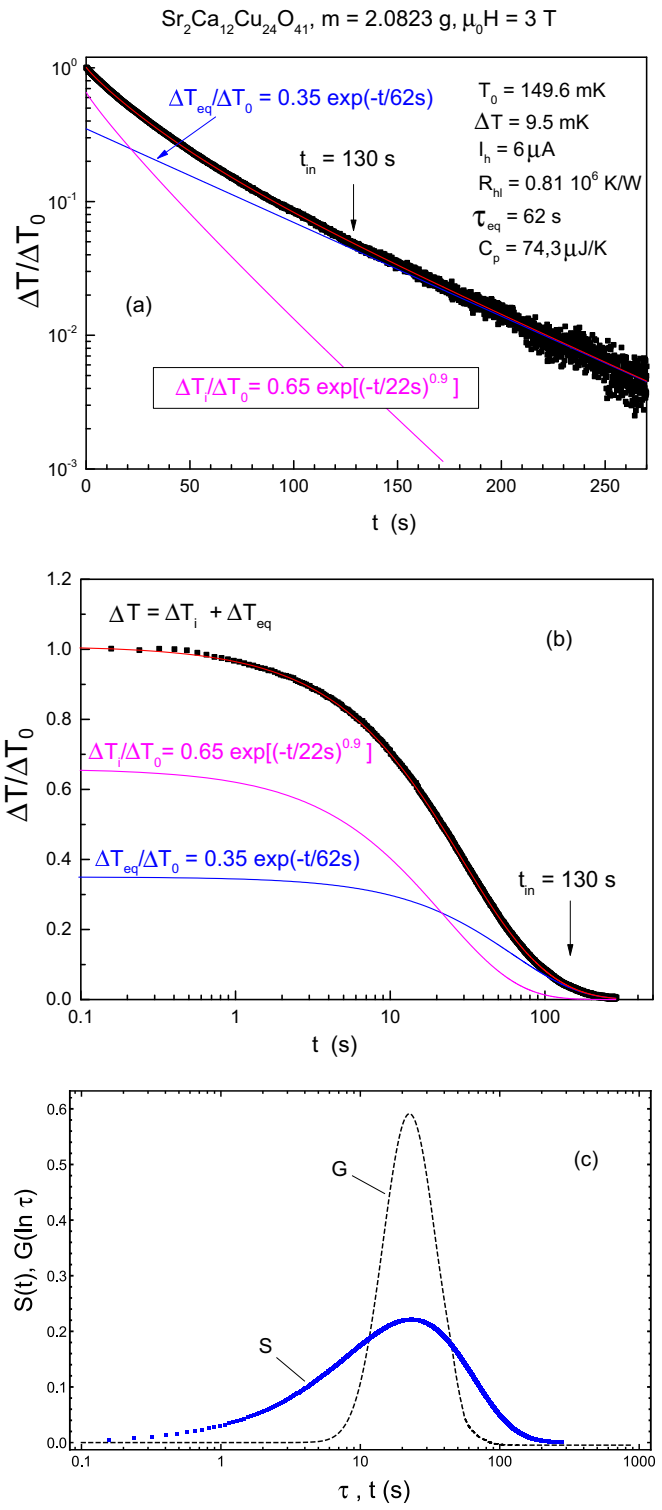

FIG. 11. A constant power of the sample heater is switched off at $t = 0$ after the waiting time $t_w = 2t_{\rm in}$ and the temperature relaxes from 160.1 to 149.6 mK. Figures 11(a) and 11(b) show the measured thermal relaxation $\Delta T(t)/\Delta T_0$ as a function of time in different semilog presentations. The inner relaxation process is finished at $t_{\rm in} = 130$ s. The thermal relaxation follows Eq. (4) at longer time $t > t_{\rm in}$ with the quasiequilibrium relaxation time $\tau_{\rm eq} = 62$ s [see Fig. 11(a)]. An additional thermal relaxation term $\Delta T_i/\Delta T_0$ is observed at $t < t_{\rm in}$ due to some inner relaxation process. We get a good fit of this term by a stretch exponential law with an exponent $\beta = 0.9$. This demonstrates that the width of the distribution function of relaxation time is small since $\beta = 1$ corresponds to the case of a Delta function $\delta(\tau_m)$. The measured inner thermal relaxation $\Delta T_i/\Delta T_0$ is shown in Fig. 11(c) (blue points) in the presentation $d(\Delta T_i/\Delta T_0)/d(\ln t)$ as a function of time for the data shown in Figs. 11(a) and 11(b). This gives roughly the distribution function of relaxation time (see the text). The numerical calculation of $\Delta T_i/\Delta T_0$ with Eq. (2) yields a Gaussian distribution (dashed curve) with nearly the same position of the maximum τ_m.

field (see Fig. 7). In addition, the temperature dependence of τ_{ms} is nearly constant below 0.1 K, thus indicating that some tunneling process starts instead of the thermal activation.

C. $Sr_2Ca_{12}Cu_{24}O_{41}$

The heat capacity is shown in Fig. 10 as a function of the temperature for different magnetic field strengths. The data are obtained by the pulse technique. The magnetic field was directed perpendicular to the c axis. A magnetic ordering is observed at 2.8 K. The heat capacity is determined below this temperature by a T^3 term (phonons and magnons), a quasilinear term, and a Schottky term. A gap opening is observed for the quasilinear term between 0 and 2 T. In particular, this leads to a crossing of the curves for 0 and 2 T (see Fig. 10). Gap values are also given in Fig. 10 (for more details, see Ref. [10]).

As in the previous case, the Schottky term is time dependent. Figure 10 shows the equilibrium heat capacity only. The condition $\tau_{\rm eq} > t_{\rm in}$ is satisfied for all the experimental values of temperature and magnetic field due to the high background heat capacity and the large sample mass. We fit the Schottky term with the amplitude of the $Sr_{14}Cu_{24}O_{41}$ sample since the maximum is at lower temperatures. We get a good fit to the data (see solid lines in Fig. 10). The Schottky energy is the last free parameter and it is also given in Fig. 10. The Schottky energy depends only weakly on the magnetic field (a roughly linear dependence) in difference to the other two materials.

The parameters of thermal relaxation at 0.1 K and different magnetic field strengths are given in Table II, where $\Delta T_{\rm eq}$ is subtracted. At high temperature, this contribution is relatively large and does not yield the accurate amplitude of the distribution function. However, this can be easily corrected as we have found that the distribution function is determined by one Gaussian only with both magnetic field and temperature-independent width w [see Fig. 11(c) where dots show $d(\Delta T_i/\Delta T_0)/d(\ln t)$ and dashed lines show the Gaussian function]. Similarly we obtain the distribution function at 10 T and different temperatures (see Fig. 12). The width of the distributions remains always constant ($w = 0.5$). Thus the maximum of the distribution shifts with magnetic field and/or temperature. This parameter is given in Fig. 13 as a function of $1/T$ for different magnetic field strengths. In contrast to the other two materials, the activation energy is not a constant but increases with increasing magnetic field. Deviations from the Arrhenius law are found at low temperatures. The curves are calculated using Eq. (10),

$$\tau^{-1} = \tau_{ta}^{-1} + \tau_{\rm tun}^{-1}, \qquad (10)$$

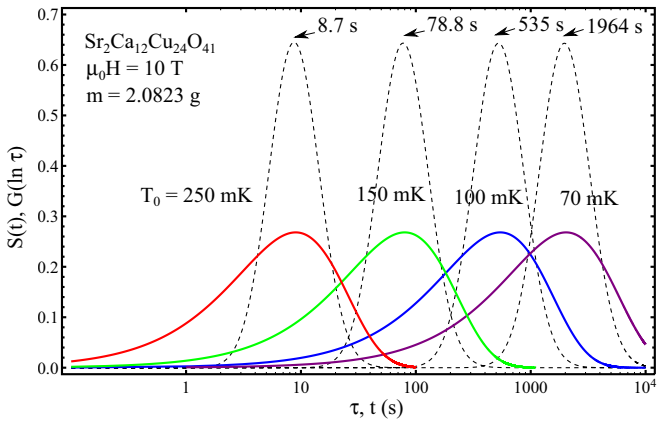

FIG. 12. The measured inner thermal relaxation $\Delta T_i/\Delta T_0$ in the presentation $d(\Delta T_i/\Delta T_0)/d\ln t$ as a function of time at 10 T and different temperatures. The dashed curves show the distribution function obtained by the calculation of ΔT_i with Eq. (2). The width of the distribution function is independent from the magnetic field and temperature ($w = 0.5$). The temperature and magnetic field dependence of τ_m (the position of the maximum) is given in Fig. 13.

with the relaxation time of the thermal activated process

$$\tau_{ta} = \tau_0 \exp\left[\frac{E_a(H)}{k_B T}\right] \tag{11}$$

and the relaxation time of tunneling

$$\tau_{\text{tun}} = \frac{\tau_{\text{tun}}(0.1\text{K})}{(T/0.1\text{K})^3}, \tag{12}$$

$\tau_{\text{tun}}(0.1K) = 70\exp(0.21\mu_0 H)$ s, where $\mu_0 H$ is in Tesla units. Both fitting parameters, E_a and $\ln[\tau_{\text{tun}}(0.1\text{K})]$, are proportional to the magnetic field. This is not surprising since both values are proportional to the barrier height. We get for the activation energy

$$E_a/k_B = [0.79 + 0.017(\mu_0 H)]\text{K}, \tag{13}$$

where $\mu_0 H$ is in Tesla units.

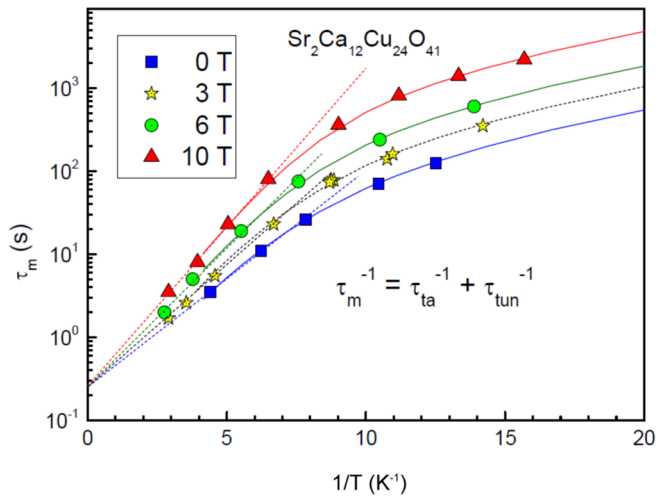

FIG. 13. The Arrhenius plot of the peak position in the distribution function for different magnetic field. The activation energy increases with increasing magnetic field. Tunneling is observed at low temperatures. The curves are calculated for a relaxation rate determined by tunneling and thermal activated processes.

IV. DISCUSSION

The heat capacity is found to be very similar for all investigated materials with CDW or SDW: it is proportional to T^{-2} and strongly time dependent. However, the behavior of the relaxation-time spectrum is very different for different materials: the distribution function contains one or two Gaussians, the width of the distribution is either a constant or dependent on the magnetic field, the relaxation time is usually caused by a thermal activation process, but in some materials tunneling seems to be possible at very low temperatures.

The analysis of the relaxation-time spectra allows us to determine the distribution functions for all three materials. They demonstrate a rather specific behavior which gives an important information on the low-temperature ground state and collective effects.

First of all, the experimental data for $(TMTTF)_2Br$ confirm the previous results in Ref. [7] and give a better understanding of the magnetic-field-induced density-wave glass state observed in Ref. [6]. In particular, the distribution function is found to have a broad shape with low barrier height. At the same time, no tunneling process was observed. This means that there are a number of metastable states but the tunneling mass turns out to be large. The increasing magnetic field markedly shifts the position of the maximum (quadratic in H) while the width of the distribution function remains almost the same. What is important is that the activation energy does not depend on the magnetic field.

The long-time thermal relaxation in $Sr_{14}Cu_{24}O_{41}$ shows different behavior. The distribution function includes two well-defined narrow Gaussian peaks of different height. This indicates the presence of two types of relaxing structures. We observed a distinct difference in their behavior. The higher barriers show both thermal activation and tunneling processes. They are weakly sensitive to the magnetic field. For lower barriers the relaxation time is caused by a thermal activation process only. The activation energy does not depend on H. As was mentioned in the introduction, this material develops the CDW ground state at low temperatures. Notice that according to the model of Larkin [14] and Ovchinnikov *et al.* [15] the low-energy excitation appears as a consequence of pinning the CDW (or SDW) to defects. The strong impurity pinning leads to a generation of bisolitons, pairs of solitons, and an antisoliton [6]. Our study shows that there are two kinds of the effective two-level systems (TLSs) having a different origin. The nature of these states is still an open question.

One of the most interesting results is the drastic change of the relaxation-time spectrum in $Sr_{14}Cu_{24}O_{41}$ after doping the material with Ca: the maximum changes by a factor of 600 (see Fig. 14). The distribution is represented by a single narrow Gaussian function. The relaxation includes both thermal and tunneling processes. A strong dependence on the magnetic field is found: we observed the exponential growth of the relaxation time due to a linear increase of the activation energy with H. Trying to understand such behavior, which differs

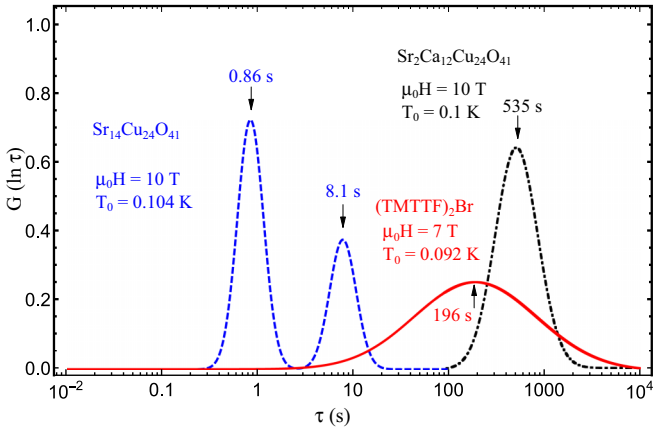

FIG. 14. The distribution function of the relaxation time obtained for the three different materials at nearly the same temperature and high magnetic field. The doping of $Sr_{14}Cu_{24}O_{41}$ with Ca shifts the distribution function to much longer time.

markedly from both previous materials, let us recall that there is a principal difference between the low-temperature ground states of $Sr_{14-x}Ca_xCu_{24}O_{41}$ with $x = 0$ and 12. For $x = 0$, the low temperature phase of the chains is a 2D antiferromagnetic (AF) dimer and complementary charge order while for ladders it is the gapped spin-liquid and 2D CDW order. In case of $x = 12$, the AF order is established both for the chains and the ladders [9]. Therefore, the possible low-energy excitations of $Sr_2Ca_{12}Cu_{24}O_{41}$ can be implemented through AF SDW transition followed by the Larkin-Ovchinnikov scenario of pinned SDW with the formation of bisolitons. The magnetic origin of bisolitons could explain the observed noticeable reaction to the magnetic field. This observation agrees with the findings in Ref. [16] where the low-temperature magnetic response of these compounds is expected to be determined by the weakly coupled CuO_2 spin chains. A reduction of the number of holes in the chains through Ca doping leads to an additional contribution to the magnetization, which depends linearly on the magnetic field. What is important is that the magnetization is found to be almost isotropic. In our experiments we directed H either along or normal to the *c* axis.

Notice that the narrow peak assumes the well-defined effective two-level systems, which supports the bisoliton picture with exactly two metastable states. This differs from the situation in $(TMTTF)_2Br$ where presumably several metastable states appear due to local deformations of the SDW. The higher barriers in comparison to both $(TMTTF)_2Br$ and $Sr_{14}Cu_{24}O_{41}$ can be explained as a result of a structural evolution. Indeed, it was found in [17] that Ca doping increases the interaction between the two chain and ladder sublattices. According to the theoretical models in Refs. [14,15], the barrier height grows with the interaction energy between chains.

For comparison, the most important physical parameters obtained in our experiments are given in Table III together with the results of Ref. [2]. Notice a remarkable change of the activation energy E_a while its magnetic field dependence was observed in $Sr_2Ca_{12}Cu_{24}0_{41}$ only. The value of τ_0 has the same order at zero field. For $(TMTTF)_2Br$ it changes from 1 to 2.7 s due to a phase transition and strong magnetic field dependence was observed. In other materials, no field dependence was found. τ_m does not depend on the magnetic field in $Sr_{14}Cu_{24}O_{41}$ and is found to be strongly dependent in two other materials. It should be noted that the origin of this dependence is different: it changes through τ_0 in $(TMTTF)_2Br$ and due to E_a in $Sr_{14}Cu_{24}O_{41}$. E_s is small in all investigated materials. Notice that $Sr_{14}Cu_{24}O_{41}$ is the first CDW/SDW system where the maximum of the Schottky term was observed. It is necessary to determine the absolute value of this contribution. Seemingly, there is a different magnetic field dependence for CDW (as H^2) and SDW (linear in H). Unfortunately, there is no chance to find the maximum of the heat capacity for incommensurate SDW systems since even at 10 T it lies below 100 mK where τ_m exceeds 10^7 s. A similar situation takes place in the spin ice $Dy_2Ti_2O_7$: below 0.4 K an additional time-dependent contribution to the heat capacity was observed, which could be the upper tail of a Schottky contribution. The inner thermal relaxation follows the Arrhenius law with a much larger activation energy $E_a/k_B =$ 9.8 K (see Ref. [8]). The relaxation time is around 60 000 s at 0.34 K and becomes too large below 0.3 K to determine experimentally the equilibrium heat capacity. The amplitude A_s in $Sr_{14}Cu_{24}O_{41}$ and $Sr_2Ca_{12}Cu_{24}0_{41}$ (roughly one defect per two unit cells) is much smaller than in $(TMTTF)_2Br$ (six defects per unit cell). A similar value was estimated from heat release data in $(TMTTF)_2PF_6$ (one defect per four unit cells, see Refs. [5,7]). This large number is an indication that impurities are not the origin of TLSs.

Finally, let us compare the obtained distribution functions to those in other materials. For example, in structural glasses there was obtained a broad distribution in energy from 0 to k_BT and a broad distribution in τ: $\Delta(\ln\tau) = \ln(\tau_{\max}/\tau_{\min})$ is found to have a value of about 50 for vitreous silica [18]. In CDW/SDW systems the distribution in E is a Delta function with a very low E_s. This indicates the presence of well-defined TLSs without any distribution. The distribution in τ is very small in comparison to a glass [$\Delta(\ln\tau) = 3$ for $(TMTTF)_2Br$ and is equal to 1 for the other two investigated systems]. In addition, there is a precise barrier height with some broadening. From this point of view, these materials are not glasses.

V. CONCLUSION

The most important result of the paper is the determination, for the first time, of the distribution functions of relaxation times in systems with charge- or spin-density wave. As we have shown, this became possible by investigation of the thermal relaxation from a thermal equilibrium state at T_1 to another one at T_0 provided that the maximum time for inner relaxation t_{in} is not too long. It has been found that a commonly used description based on the relaxation rate does not give the proper distribution function even in the case of a broad distribution (see TMTTF at short time). For the correct determination of the relaxation-time distribution we have performed numerical calculations.

We found the explicit form of distribution functions for three different materials with the result that they correspond to one or two Gaussian functions. A comparison of the temperature and magnetic field dependence of the relaxation-time spectrum shows that the behavior is very different for

TABLE III. Most important parameters.

CDW/SDW	$(TMTTF)_2PF_6$ SDW	$(TMTTF)_2Br$ SDW	$Sr_{14}Cu_{24}O_{41}$ CDW	$Sr_2Ca_{12}Cu_{24}0_{41}$ SDW
E_a/k_b (K)	1.7 [2]	0.51[a]	0.2	0.8–1.0[b]
$\tau_0(0\,T)$ (s)	0.42[c]	0.05[a]	0.2 and 0.5	0.3
$\tau_0(10\,T)$ (s)		1.55	0.2 and 0.5	0.3
$\tau_0(\mu_0 H > 4\,T)$		$\propto H$	const.	const.
$\tau_m(0.1\,K,0\,T)$ (s)	10^7[c]	7.8	0.86 and 8.1	63
$\tau_m(0.1\,K,10\,T)$ (s)		242[d]	0.86 and 8.1	535
$E_s(4\,T)/k_B$ (mK)		<52	40	<35
$E_s(\mu_0 H > 4\,T)$ (K)		$\propto H$	$\propto H^2$	$\propto H$
A_s (J/mol K)		>50.5	3.9	>3.9

[a]For field induced phase.
[b]Magnetic-field dependent.
[c]Calculated from the maximum of the relaxation-time spectrum at 0.2 K in Ref. [2].
[d]Estimated with Eq. (8).

studied materials. For $(TMTTF)_2Br$ no tunneling process was observed while in two other materials both thermal and tunneling processes were revealed. We found a different reaction to the magnetic field: while the Schottky energy is found to have the same order of magnitude for all three materials (below 100 mK even at high magnetic field 10 T), it behaves as H^2 in TMTTF and Sr, but is linear in H for Ca. It should be also emphasized that the amplitude of the Schottky term, which is expected to be proportional to the number of pinning centers of the SDW or CDW [15], turns out to be too large in $(TMTTF)_2Br$ and more than ten times smaller in $Sr_{14}Cu_{24}O_{41}$ and $Sr_2Ca_{12}Cu_{24}O_{41}$. This leads to the conclusion that low-temperature anomalies in these materials are not universal.

The most interesting experimental results concern $Sr_2Ca_{12}Cu_{24}O_{41}$. The fact is that the resistivity measurements reveal neither CDW nor SDW contribution at high Ca concentrations (see, e.g., Ref. [9]). Our experiments clearly show the relaxation process which includes both thermal activation and tunneling, thus favoring the AF SDW transition in $Sr_2Ca_{12}Cu_{24}O_{41}$ at low temperatures. Notice that the resistivity measurements were performed at higher temperature and our method is much more sensitive. We expect that the more precise resistivity measurements must reveal the SDW contribution.

The explicit form of the distribution function gives us important information about the structure of the ground state and low-energy excitations in these materials. The theoretical model with two metastable states (SDW and bisolitons) gives reasonable explanation of our results for $Sr_2Ca_{12}Cu_{24}O_{41}$. In case of CDW compound $Sr_{14}Cu_{24}O_{41}$, there appears an additional peak indicating the presence of two kinds of the effective two-level systems having a different origin. The more complex situation takes place in $(TMTTF)_2Br$ where the distribution function has a broad shape with low barrier height. There occur several metastable states in the SDW ground state. This case is beyond the theoretical description in Refs. [14,15] and needs additional analysis. Perhaps this explains why the estimated number of pinning centers of the SDW is too large in this material.

As the main conclusion, the investigation of the long-time thermal relaxation yields more detailed information about the relaxation-time spectrum, which leads after more systematical investigations to a better understanding of the low-energy excitations in systems with CDW or SDW.

ACKNOWLEDGMENTS

We acknowledge the support of the European Community Research Infrastructures under the FP7 Capacities Specific Program, MICROCELVIN Project No. 228464, and Landau-Heisenberg Program No. HLP-2016-26.

[1] J. C. Lasjaunias, K. Biljakovic, and P. Monceau, Phys. Rev. B **53**, 7699 (1996).
[2] J. C. Lasjaunias, R. Melin, D. Staresinic, K. Biljakovic, and J. Souletie, Phys. Rev. Lett. **94**, 245701 (2005).
[3] J. C. Lasjaunias, K. Biljakovic, S. Sahling, and P. Monceau, J. Phys. IV (France) **131**, 193 (2005).
[4] J. C. Lasjaunias, S. Sahling, K. Biljakovic, and P. Monceau, J. Magn. Mat. **290-291**, 989 (2005).
[5] S. Sahling, J. C. Lasjaunias, K. Biljakovic, and P. Monceau, J. Low Temp. Phys. **133**, 273 (2003).
[6] R. Melin, J. C. Lasjaunias, S. Sahling, G. Remenyi, and K. Biljakovic, Phys. Rev. Lett. **97**, 227203 (2006).
[7] S. Sahling, J. C. Lasjaunias, R. Melin, P. Monceau, and G. Remeyi, Eur. Phys. J. B **59**, 9 (2007).
[8] D. Pomaranski, L. R. Yaraskavitch, S. Meng, K. A. Ross, H. M. L. Noad, H. A. Dabkowska, B. D. Gaulin, and J. B. Kycia, Nat. Phys. **9**, 353 (2013).
[9] T. Vuketic, B. Korin-Hamzic, T. Ivek, S. Tomic, B. Gorshunov, M. Dressel, and J. Akimitsu, Phys. Rep. **428**, 169 (2006).
[10] S. Sahling *et al.* (unpublished).

[11] L. Lundgren, P. Svedlindh, P. Nordblad, and O. Beckman, Phys. Rev. Lett. **51**, 911 (1983).
[12] O. Bèthoux, R. Brusetti, J. C. Lasjaunias, and S. Sahling, Cryogenics **35**, 447 (1995).
[13] S. Sahling, G. Remenyi, C. Paulsen, P. Monceau, V. Saligrama, C. Marin, A. Revcolevschi, L. P. Regnault, S. Raymond, and J. E. Lorenzo, Nat. Phys. **11**, 255 (2015).
[14] A. I. Larkin, Zh. Eksp. Teor. Fiz. **105**, 1793 (1994) [JETP **78**, 971 (1994)]
[15] Yu. N. Ovchinnikov, K. Biljakovic, J. C. Lasjaunias, and P. Monceau, Europhys. Lett. **34**, 645 (1996).
[16] R. Klingeler, N. Tristan, B. Büchner, M. Hücker, U. Ammerahl, and A. Revcolevschi, Phys. Rev. B **72**, 184406 (2005).
[17] G. Deng, V. Pomjakushin, V. Petricek, E. Pomjakushina, M. Kenzelmann, and K. Conder, Phys. Rev. B **84**, 144111 (2011).
[18] S. Sahling, S. Abens, and T. Eggert, J. Low Temp. Phys. **127**, 215 (2002).